Oscillatory behavior of interlayer Dzyaloshinskii-Moriya interaction by spacer thickness variation

E. Demiroglu [1], K. Hancioglu,[1] I. Yavuz,[1] C. O. Avci [2], and C. Deger [1,*]
[1]*Department of Physics, Marmara University, 34722, Ziverbey, Istanbul, Turkiye*
[2]*Institut de Ciència de Materials de Barcelona (ICMAB-CSIC), Campus de la UAB, 08193 Bellaterra, Spain*

(Received 2 December 2023; revised 26 March 2024; accepted 27 March 2024; published 24 April 2024)

The interlayer Dzyaloshinskii-Moriya interaction (IL-DMI) has recently emerged as an ingredient promoting chiral orthogonal coupling between adjacent magnetic layers in multilayered systems. IL-DMI offers an additional tuning knob to engineer the magnetic behavior in spintronic devices, which could be useful for nonvolatile logic and memory technologies. Here, we systematically study, via first-principles calculations and the three-site Fert-Lévy model, the spacer thickness dependence of the IL-DMI between an out-of-plane ferrimagnet TbCo and an in-plane ferromagnet Co through Pt, Ir, Pd, and Ru. We observed a damped oscillatory behavior with increasing spacer thickness in all cases with characteristic amplitude and periodicity. Furthermore, we established a direct correlation between the IL-DMI and density of states of bottom and top Co atoms, dominated by the spacer thickness, which is attributed to a hybridization of electronic orbitals. Based on this compelling evidence, we propose that the electronic orbital hybridization contributes to the microscopic origin of the IL-DMI metallic magnetic multilayers. We anticipate that our results will provide insights into the understanding and precise control of IL-DMI in a wide range of materials and spintronic device concepts.

DOI: 10.1103/PhysRevB.109.144422

I. INTRODUCTION

Interlayer exchange coupling in magnetic multilayers is a central topic in condensed matter physics and materials science [1,2]. It allows us to engineer the magnetic behavior in multilayered systems, not easily achievable in individual constituents. Most prominent coupling mechanisms include direct coupling [e.g., between an antiferromagnet(AFM) and ferromagnet(FM)] or indirect coupling mediated through Ruderman-Kittel-Kasuya-Yosida (RKKY) interactions between FM layers through a nonmagnetic(NM) spacer [3–6]. Both types of interactions generally give rise to symmetric exchange, i.e., either parallel or antiparallel configuration of the adjacent layers. Recently, a kind of interlayer exchange coupling driven by the interlayer Dzyaloshinskii-Moriya interaction (IL-DMI) has been theoretically [7] and experimentally discovered [8,9]. The IL-DMI leads to asymmetric coupling, promoting perpendicular alignment of the neighboring magnetic layers with well-defined chirality [10]. The IL-DMI is phenomenologically like the well-known intralayer DMI, which is capable of stabilizing topologically protected chiral two-dimensional (2D) and three-dimensional (3D) spin textures in single magnetic layers [11,12]. However, the manifestation of IL-DMI is fundamentally different than the intralayer DMI as it acts globally on uniform magnetizations and hence offers opportunities for magnetic manipulation in multilayers in a device context [13,14].

The IL-DMI is first revealed by the existence of a chiral exchange bias at room temperature in ultrathin asymmetric synthetic AFM bilayers [8]. It is commonly facilitated through a paramagnetic heavy metal(HM) in systems that lack inversion symmetry [15]. The symmetry-breaking effect is ascribed to the appearance of noncollinear spin modulation, influenced by distinct IL-DMI profiles during magnetic reversal. Although the IL-DMI may initially appear insufficient to significantly modify the intralayer magnetic ordering, given the competition with robust direct exchange and intralayer DMI contributions, it has proved its effectiveness in contending with RKKY coupling, thereby exerting influence on the interlayer ordering [9,13,16]. Consequently, IL-DMI induces tilted magnetic structures along the film normal, leading to chiral exchange-biased hysteresis loops in such systems. The presence of IL-DMI was recently discovered in FM/NM/FM trilayers with different spacer elements, including Ru [8,9,17], Pt [10], Pd [18], Ir [19], and Ag [20]. In the Pt spacer case, the IL-DMI strength decreased monotonically with increasing thickness, while the decrease in Ru, Ir, and Ag cases follows an oscillatory fashion. Furthermore, the oscillatory behavior of IL-DMI changes its sign for the Ag spacer, while it oscillates in the same sign and direction for the Ru and Ir spacers. The reason for these differences may be that each spacer element mediates IL-DMI between the magnetic layers differently, or these differences may occur due to the imperfect nature of the experiments, such as the inevitable presence of crystalline defects, roughness, and uniaxial magnetic anisotropy in the magnetic layers. The role of the spacer on the sign and strength of IL-DMI is still in comprehensive and needs further research.

In this paper, we simulated the spacer layer thickness dependence of the IL-DMI between an out-of-plane ferrimagnet TbCo and in-plane FM Co through various spacer layer elements by the three-site Fert-Lévy model. We first obtained out-of-plane TbCo by crystal strain engineering. We

*caner.deger@marmara.edu.tr

then varied the Pt spacer thickness and found an RKKY-type damped oscillatory behavior. The direction of IL-DMI was also changed by the spacer thickness. The variation in the strength of IL-DMI is microscopically linked to the hybridization between bottom and top Co atoms via the Pt spacer by analyzing the element-resolved density of states(DOS) around the Fermi level. We further extend our computations to reveal the effect of different spacer elements, Ru, Pd, and Ir, and find that the IL-DMI is operative in all these spacer layers with distinct amplitude and oscillation frequencies. We anticipate that our predictions will provide insights into the control of the IL-DMI for future spintronic memory and logic devices and stimulate further research into its microscopic origins and engineering.

II. METHODOLOGY

IL-DMI calculations were conducted using the constrained spin method implemented in VASP [21,22]. This method has been previously employed for DMI calculations in various contexts, including bulk frustrated systems, insulating chiral-lattice magnets, and ultimately, FM/HM interfaces [23–26]. The calculations utilized the generalized gradient approximation of the Perdew-Burke-Ernzerhof type functional to account for electron-electron interactions [27,28]. The projector augmented-wave method was employed to handle electron-ion interactions [29]. The cutoff energies for the plane-wave basis sets were set at 400 eV. The crystal structure of the TbCo layer has hexagonal close-packed stacking with ABA sequence. The Pt spacer and top Co layer have face-centered cubic structure with the same sequence. The *Fd*3*m* [227] space group of TbCo perfectly matches with the *Fm*3*m* [225] space group of Pt and Co. The resulting total structure is a rhombohedral stacked trilayer along the(111) direction. A vacuum slab with a thickness of 8 monolayers (ML) was included along the thickness direction to prevent interactions between the repeating slabs. Here,Γ-centered Monkhorst-Pack $8 \times 8 \times 1$ k-point sampling is used for the Brillouin zone mesh, which is considered adequate for achieving convergence. Structural relaxation is carried out until the forces reach a magnitude <1 meV/Å to attain the most stable geometry. The convergence criterion was set as 10^{-6} eV in total energy for electronic steps. Subsequently, we calculated the electronic charge distribution of the structure by solving the Kohn-Sham equations without considering spin-orbit coupling(SOC). Finally, we constructed clockwise (CW) and counterclockwise (CCW) rotations, considering the relative orientation of the bottom TbCo and the top Co, using the constrained spin method [30]. The IL-DMI energy is assessed using the total energies for CW and CCW configurations. The self-consistent total energy difference between these two configurations is employed to calculate the IL-DMI in the presence of SOC by using the equation [19]:

$$E^{\text{tot}} = \mathbf{D}_{\text{IL-DMI}} \cdot (\mathbf{S}_{\text{Co}} \times \mathbf{S}_{\text{TbCo}}) + E_{\text{other}}, \tag{1}$$

where $\mathbf{S}$ denotes the spin vector, and E_{other} comprises symmetric exchange and anisotropy contributions. We fix $\mathbf{M}_{\text{TbCo}}$ parallel to the z axis, while $\mathbf{M}_{\text{Co}}$ lies along the x axis.

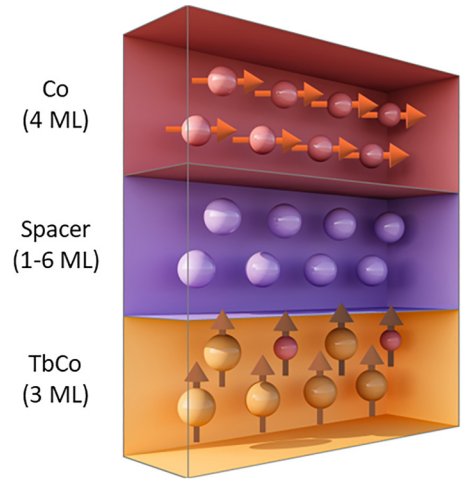

FIG. 1. Schematics of the model TbCo (3 ML)/spacer/Co (4 ML) structure where the spacer thickness is varied from 1 to 6 ML. The direction of the magnetic moments of the bottom TbCo layer is fixed in the z direction ($\mathbf{M}_{\text{TbCo}} \parallel \mathbf{z}$), while that of the top Co layer is fixed sequentially in the x ($\mathbf{M}_{\text{Co}} \parallel \mathbf{x}$) and $-x$ ($\mathbf{M}_{\text{Co}} \parallel -\mathbf{x}$) directions to construct an orthogonal magnetic configuration and determine the preferred chirality for each spacer thickness value.

The chirality-dependent energy difference of magnetic layers is calculated by evaluating the energy difference between spin configurations with opposite chirality along the z axis. The computational details of the magnetic anisotropy energy(MAE) calculations can be found in the Supplemental Material [31] (including Refs. [32,33]).

III. RESULTS AND DISCUSSION

A. Perpendicular magnetic anisotropy in TbCo

We chose TbCo/spacer/Co-type heterostructures (see Fig. 1) to study the IL-DMI. TbCo as a bottom layer is convenient since it has a natural in-plane inversion symmetry breaking and high SOC. Before modeling the full structure, we first ensured the perpendicular magnetic anisotropy(PMA) of the TbCo layer. We found that the relaxed geometry of TbCo possesses an in-plane magnetic anisotropy. It was reported that the PMA of TbCo strongly depends on the magnetostriction and the planar stress in the crystal [34]. Thus, we examined the effect of magnetostriction on PMA in a 3 ML TbCo slab by varying crystal lattice strain, as shown in Fig. 2. A positive MAE indicates that the easy-axis of the system is out-of-plane. The top and side views of the hexagonal lattice can be seen in Figs. 2(b) and 2(c), respectively. The relaxed geometry corresponds to the $c/a = 1$ ratio in the hexagonal lattice of TbCo. The blue gradient in the background indicates the relative formation energy of the strained crystal. The amount of energy required to obtain the maximum applied strain value ($c/a = 0.92$) is only 0.56 eV above the relaxed geometry. This energy is comparable with the energy required to apply a similar amount of strain to the Pt/Co interface [12]. The relaxed geometry of TbCo, isolated from any external or growth-induced stress, has a weak in-plane magnetic anisotropy. Any compressive strain forces the magnetic easy axis of the system to be out-of-plane with a

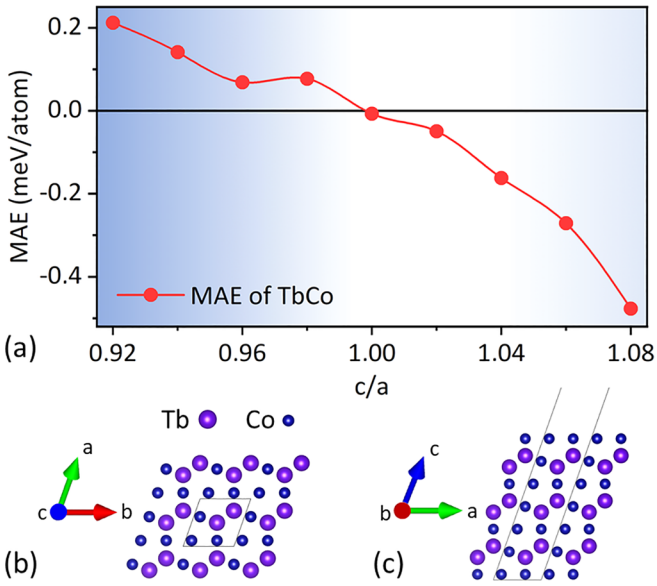

FIG. 2. Perpendicular magnetic anisotropy (PMA) of TbCo. (a) The dependence of the magnetic anisotropy energy (MAE) of the TbCo layer on the ratio of lattice parameters c/a. The background gradient shows the formation energy relative to the optimized geometry. The maximum relative formation energy indicated by blue region at the left end of the figure is 0.56 eV. A positive value of MAE indicates a PMA for TbCo. (b)and (c) Top and side views of TbCo crystal.

positive MAE value. This finding is in agreement with the experimental work performed by Yoshino *et al.* [34]. On the other hand, a tensile strain ($c/a > 1$) causes a strong in-plane anisotropy. We should note that the maximum tensile strain can be achieved by a small amount of energy 0.1 eV. In light of this discussion, we choose a compressive strain of 6% ($c/a = 0.94$) to model the perpendicularly magnetized TbCo layer for this paper. The amount of energy required to achieve this strain is 0.34 eV. This lattice strain results in a reasonable MAE value of 0.14 eV and can be obtained by employing proper substrates and/or buffer layers.

B. Pt thickness dependence of IL-DMI in TbCo/Pt/Co trilayers

We built Pt(x ML)/Co (4 ML) bilayer on the TbCo structure with the aforementioned lattice strain and performed geometry optimizations by fixing TbCo atoms. This approach allows us to mimic the effect of the buffer layer or substrate on the crystallization manner and retain the strain-induced PMA of the TbCo layer. The Pt spacer thickness is varied from 1 to 6 ML. We employed 4 ML of Co for the top layer to construct an orthogonal magnetization. In Fig. 3, we report the spacer thickness dependence of the IL-DMI as a function of the Pt spacer thickness. Positive IL-DMI values (red background) represent a chirality that favors the configurations ($\mathbf{M}_{\mathrm{TbCo}} \parallel \mathbf{z}$, $\mathbf{M}_{\mathrm{Co}} \parallel -\mathbf{x}$) and ($\mathbf{M}_{\mathrm{TbCo}} \parallel -\mathbf{z}$, $\mathbf{M}_{\mathrm{Co}} \parallel \mathbf{x}$), while negative IL-DMI values (blue background) correspond to a chirality that favors the configurations ($\mathbf{M}_{\mathrm{TbCo}} \parallel \mathbf{z}$, $\mathbf{M}_{\mathrm{Co}} \parallel \mathbf{x}$) and ($\mathbf{M}_{\mathrm{TbCo}} \parallel -\mathbf{z}$, $\mathbf{M}_{\mathrm{Co}} \parallel -\mathbf{x}$). For the sake of the discussion, we will call the positive and negative values CCW and CW, respectively. At the lowest Pt thickness, the

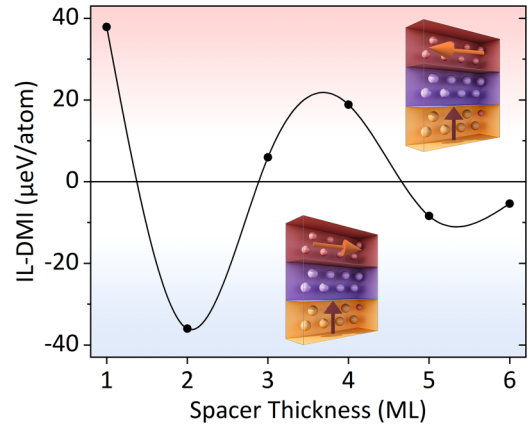

FIG. 3. Interlayer Dzyaloshinskii-Moriya interaction (IL-DMI) in the TbCo/Pt/Co multilayer structure. The variation of IL-DMI between TbCo and Co layers is given with respect to Pt spacer thickness. Positive IL-DMI values with red background indicate that the favorable configurations are ($\mathbf{M}_{\mathrm{TbCo}} \parallel \mathbf{z}$, $\mathbf{M}_{\mathrm{Co}} \parallel -\mathbf{x}$) and ($\mathbf{M}_{\mathrm{TbCo}} \parallel -\mathbf{z}$, $\mathbf{M}_{\mathrm{Co}} \parallel \mathbf{x}$), while negative IL-DMI values with blue background denote that the favorable configurations are ($\mathbf{M}_{\mathrm{TbCo}} \parallel \mathbf{z}$, $\mathbf{M}_{\mathrm{Co}} \parallel \mathbf{x}$) and ($\mathbf{M}_{\mathrm{TbCo}} \parallel -\mathbf{z}$, $\mathbf{M}_{\mathrm{Co}} \parallel -\mathbf{x}$).

IL-DMI has a strong CCW chirality of 37.8 μeV/atom. It then changes sign in an oscillatory fashion while attenuating toward the 6 ML Pt spacer thickness. This confirms that the coupling between bottom TbCo and top Co layers should disappear for a sufficiently thick NM spacer; however, the spacer thickness is limited to 6 ML due to the logarithmically increasing computational cost with enlarging supercell. The damped oscillatory behavior of IL-DMI of the Pt spacer thickness is in contrast with recent experimental studies, which suggest a quasimonotonic decay with increasing Pt thickness [10,35]. This conflict can be attributed to the inevitable defects of the crystal growth process, which are prevented in the simulations, such as polycrystalline formation of the layers, the tendency of island formation of Pt, and roughness at the interface. Still, authors of several experimental works reported a damped oscillation rather than a monotonic decay for different spacer elements [19,20]. Liang *et al.* [19] reported that Ir spacer thickness variation leads to a damped oscillation in the strength of the coupling between Pt/Co bilayers, while the sign of the interaction remains intact. Likewise, Arregi *et al.* [20] observed a damped oscillatory IL-DMI between Co layers via an Ag spacer. Even if Ag is a low-SOC material, the IL-DMI measured in their trilayers is orders of magnitude larger than that of well-known high-SOC systems using HMs as a spacer. Therefore, it is worth investigating the relationship between IL-DMI and the electronic structures of the materials to get a deeper understanding of the microscopic origin of IL-DMI.

Figure 4 links the IL-DMI to the DOS of the structures. Element-resolved partial DOS of Pt spacer thicknesses of 1, 2, and 6 ML can be found in Figs. 4(a)–4(c), respectively. We only focus on the alignment of the DOS of bottom and top Co atoms near the Fermi level. From 1 to 6 ML spacer thickness, we observed a decrease in the DOS of the d bands of Co atoms. Considering that the number of Co atoms in the structure is constant for different spacer thicknesses, this

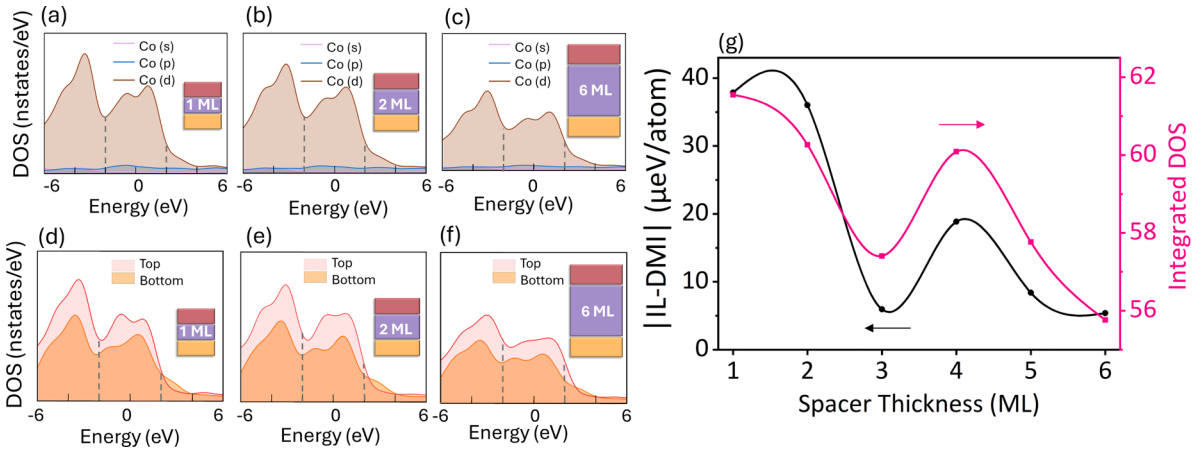

FIG. 4. Relation between interlayer Dzyaloshinskii-Moriya interaction (IL-DMI) and density of states(DOS). (a)–(c) Orbital-resolved partial DOS and (d)–(f) layer-resolved partial DOS of the structure with Pt spacer of 1, 2, and 6 ML thickness, respectively. (g) A qualitative analysis on the link between IL-DMI strength and DOS. The normalized IL-DMI strength and the integrated DOS display a strong correlation. Here, we integrated the DOS in the energy interval of −0.5 to 0.5 eV relative to the Fermi energy; however, that of −1 to 1 eV and −1.5 and 1.5 eV showed a similar trend, which can be seen in the Supplemental Material [31].

decrease indicates that the orbital hybridization around the Fermi level decreases. To investigate the contribution of each magnetic layer to the total DOS near the Fermi level, we calculated the separated partial DOS for bottom and top Co ions in Figs. 4(d)–4(f). To construct the separated DOS of bottom and top Co layers, we employed the atomic-resolved DOS method. We saw that the contribution of the bottom and top Co atoms to the DOS around the Fermi level is similar; however, the contribution to DOS from the top Co layer around the Fermi level is slightly higher than the bottom Co atoms. We attribute this difference to the fact that there are more Co atoms in the top Co layer than in the bottom one. To look at this discussion quantitatively, we calculated the integrated DOS for all thickness values in Fig. 4(g). We observed a strong correlation between the normalized IL-DMI strength and the integrated DOS. A correlation between the DOS and the RKKY interaction, as a type of long-range indirect exchange coupling, has recentlybeen suggested by analytically calculating the Green's function [36]. The amplitude of RKKY interaction is found to be proportional to the DOS at the Fermi energy. Considering that the IL-DMI is an indirect interlayer antisymmetric exchange coupling, the correlation between IL-DMI and integrated DOS may help understand the microscopic origin of this interaction by first-principles calculations. Thus, the IL-DMI mediated by low-SOC atoms can be originated by the magnetic impurity atoms in the NM spacer, a strong Rashba SOC, or the interplay of both mechanisms.

C. Spacer layer element dependence of IL-DMI

We finally discuss the spacer (and thickness) dependence of the IL-DMI by employing different spacer elements. Figure 5(a) shows the IL-DMI for Ru, Pd, and Ir spacers as a function of thickness. We reproduce the IL-DMI of the Pt spacer from the same data set asin Fig. 3 for comparison. All studied spacer elements lead to an oscillation in the sign and strength of the IL-DMI. Among these, the Ir spacer tends to remain on the positive side. This unique behavior of Ir was also observed in a recent study by Liang *et al.* [19]. Here,Ir exhibits different DMI behavior than other high-SOC materials. The chirality of the intralayer DMI of the Co/Ir interface was found to be opposite to that of Co/Pt and Co/Pd, which was attributed to some additive effects and large DMI when Co is between Pt and Ir [30]. On the other hand, Ru and Pd spacers have a similar trend, while their oscillation wavelengths are different than that of the Pt spacer. The oscillatory fashion is observed for all studied spacer elements with the attenuating behavior toward the 6 ML spacer thickness. The coupling between the bottom TbCo and top Co layers almost vanishes for a sufficient spacer thickness. To understand the differences in the behaviors among different spacers and to make a clear comparison, we performed a detailed analysis of DOS around the Fermi level. We chose the 1 ML spacer thickness, where the interaction is strongest. In Figs. 5(b)–5(e), we present the partial DOS resolved for element types. The dashed lines indicate the region corresponding to near the Fermi level between −2 and 2 eV. In this region, the partial DOS for Ru and Ir spacer layers in Figs. 5(b) and 5(c) indicates a strong hybridization between the spacer layer and magnetic layers, leadingto high IL-DMI for Ru and Ir. The DOS of Pt and Pd is concentrated far from the Fermi level in Figs. 5(d) and 5(e). Especially the contribution of Pd to the DOS near the Fermi level is small, causing a weak IL-DMI for Pd spacer. It is readily apparent that the interaction between only two magnetic layers is not sufficient to establish a relationship between IL-DMI and DOS, and the overall contribution of all magnetic and NM layers should be considered. This comparison reveals that the sign, strength, and wavelength of the IL-DMI can be tailored by both the chemical composition and the thickness of the spacer. In this paper, we thus call for further experimental investigation of the IL-DMI, especially in single-crystal systems where theoretical assumptions could be valid to a certain extent.

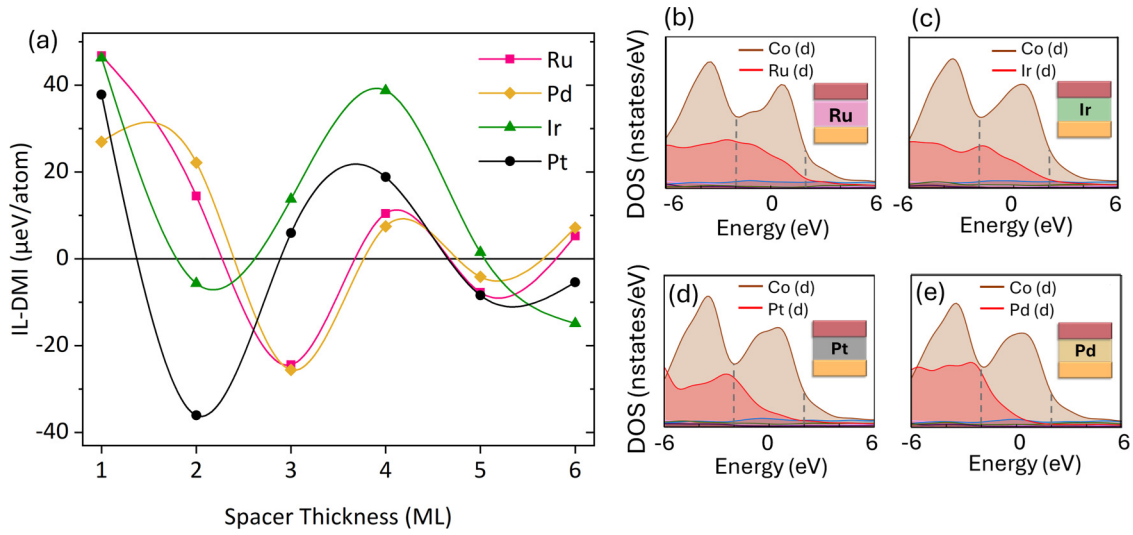

FIG. 5. Relation between interlayer Dzyaloshinskii-Moriya interaction (IL-DMI) and spacer element. (a) The spacer thickness dependence of the IL-DMI for different spacer elements. Here, IL-DMI of the Pt spacer is reproduced by the same data set as in Fig. 3, for comparison. (b)–(e) Element-resolved partial density of states for different spacers. The dashed lines indicate the region corresponding to near the Fermi level between −2 and 2 eV.

IV. CONCLUSIONS

We investigated the effect of the spacer thickness on the behavior of the IL-DMI between an in-plane Co layer and a perpendicularly magnetized TbCo layer through various spacer elements. We observed a damped oscillatory behavior with increasing spacer thickness. The electronic origin of IL-DMI was attributed to the alignment of DOS of bottom and top Co atoms, indicating an orbital hybridization around the Fermi level. Our results and the model presented will serve as a powerful tool to understand the microscopic origins of the IL-DMI and its material/thickness dependencies in a wide range of material combinations and to engineer suitable devices for next-generation spintronics.

The datasets generated and analyzed in this paper are available from the corresponding author on reasonable request.

ACKNOWLEDGMENTS

Computing resources used in this paper were provided by the National Center for High Performance Computing of Turkey under Grant No. 123N420 of The Scientific and Technological Research Council of Turkey. Computational analyses were performed at the Simulations and Modeling Research Lab, Physics Department of Marmara University. C.O.A. acknowledges funding from the European Research Council under the European Union's Horizon 2020 research and innovation programme (Project MAGNEPIC, Grant agreement No. 949052) and from the MUST project with Reference No. PCI2023-143400/MCIU/AEI/10.13039/501100011033 co-funded by the European Union. The authors thank Kerem Iscan for fruitful discussions.

[1] S. S. P. Parkin, R. Bhadra, and K. P. Roche, Phys. Rev. Lett. **66**, 2152 (1991).
[2] Y.-C. Lau, D. Betto, K. Rode, J. Coey, and P. Stamenov, Nat. Nanotechnol. **11**, 758 (2016).
[3] P. Bruno and C. Chappert, Phys. Rev. Lett. **67**, 1602 (1991).
[4] M. D. Stiles, J. Magn. Magn. Mater. **200**, 322 (1999).
[5] Q. Yang, L. Wang, Z. Zhou, L. Wang, Y. Zhang, S. Zhao, G. Dong, Y. Cheng, T. Min, Z. Hu *et al.*, Nat. Commun. **9**, 991 (2018).
[6] C. Deger, I. Yavuz, and F. Yildiz, J. Magn. Magn. Mater. **489**, 165399 (2019).
[7] E.Y. Vedmedenko, P. Riego, J. A. Arregi, and A. Berger, Phys. Rev. Lett. **122**, 257202 (2019).
[8] A. Fernández-Pacheco, E. Vedmedenko, F. Ummelen, R. Mansell, D. Petit, and R. P. Cowburn, Nat. Mater. **18**, 679 (2019).
[9] D.-S. Han, K. Lee, J.-P. Hanke, Y. Mokrousov, K.-W. Kim, W. Yoo, Y. L. Van Hees, T.-W. Kim, R. Lavrijsen, C.-Y. You *et al.*, Nat. Mater. **18**, 703 (2019).
[10] C. O. Avci, C.-H. Lambert, G. Sala, and P. Gambardella, Phys. Rev. Lett. **127**, 167202 (2021).
[11] I. A. Sergienko and E. Dagotto, Phys. Rev. B **73**, 094434 (2006).
[12] C. Deger, Sci. Rep. **10**, 12314 (2020).
[13] Y.-H. Huang, C.-C. Huang, W.-B. Liao, T.-Y. Chen, and C.-F. Pai, Phys. Rev. Appl. **18**, 034046 (2022).
[14] W. He, C. Wan, C. Zheng, Y. Wang, X. Wang, T. Ma, Y. Wang, C. Guo, X. Luo, M. E. Stebliy *et al.*, Nano Lett. **22**, 6857 (2022).
[15] S. Ding, A. Ross, R. Lebrun, S. Becker, K. Lee, I. Boventer, S. Das, Y. Kurokawa, S. Gupta, J. Yang *et al.*, Phys. Rev. B **100**, 100406(R) (2019).
[16] S.H. Schoenmaker, *The Interlayer Dzyaloshinskii-Moriya Interaction*, Master's Thesis, Eindhoven University of Technology, 2021.
[17] F. S. Gao, S. Q. Liu, R. Zhang, J. H. Xia, W. Q. He, X. H. Li, X. M. Luo, C. H. Wan, G. Q. Yu, G. Su *et al.*, Appl. Phys. Lett. **123**, 192401 (2023).

[18] S. D. Pollard, J. A. Garlow, K.-W. Kim, S. Cheng, K. Cai, Y. Zhu, and H. Yang, Phys. Rev. Lett. **125**, 227203 (2020).
[19] S. Liang, R. Chen, Q. Cui, Y. Zhou, F. Pan, H. Yang, and C. Song, Nano Lett. **23**, 8690 (2023).
[20] J. A. Arregi, P. Riego, A. Berger, and E. Y. Vedmedenko, Nat. Commun. **14**, 6927 (2023).
[21] G. Kresse and J. Hafner, Phys. Rev. B **47**, 558 (1993).
[22] G. Kresse and J. Furthmüller, Phys. Rev. B **54**, 11169 (1996).
[23] H. J. Xiang, E. J. Kan, S.-H. Wei, M.-H. Whangbo, and X. G. Gong, Phys. Rev. B **84**, 224429 (2011).
[24] J.-H. Yang, Z.-L. Li, X. Z. Lu, M.-H. Whangbo, S.-H. Wei, X. G. Gong, and H. J. Xiang, Phys. Rev. Lett. **109**, 107203 (2012).
[25] S. Zhang, J. Zhang, Q. Zhang, C. Barton, V. Neu, Y. Zhao, Z. Hou, Y. Wen, C. Gong, O. Kazakova *et al.*, Appl. Phys. Lett. **112**, 132405 (2018).
[26] A. Soumyanarayanan, R. Masapogu, A. Oyarce, A. K. C. Tan, M.-Y. Im, A. Petrović, P. Ho, K. H. Khoo, M. Tran, C. Gan *et al.*, Nat. Mater. **16**, 898 (2017).
[27] J. P. Perdew, K. Burke, and M. Ernzerhof, Phys. Rev. Lett. **77**, 3865 (1996).
[28] J. P. Perdew, A. Ruzsinszky, G. I. Csonka, O. A. Vydrov, G. E. Scuseria, L. A. Constantin, X. Zhou, and K. Burke, Phys. Rev. Lett. **100**, 136406 (2008).
[29] G. Kresse and D. Joubert, Phys. Rev. B **59**, 1758 (1999).
[30] H. Yang, A. Thiaville, S. Rohart, A. Fert, and M. Chshiev, Phys. Rev. Lett. **115**, 267210 (2015).
[31] See Supplemental Material at http://link.aps.org/supplemental/10.1103/PhysRevB.109.144422 for the computational details of the MAE and integrated DOS calculations.
[32] G. Kresse and J. Furthmüller, Comput. Mater. Sci. **6**, 15 (1996).
[33] P. E. Blöchl, Phys. Rev. B **50**, 17953 (1994).
[34] S. Yoshino, H. Takagi, S. Tsunashima, M. Masuda, and S. Uchiyama, Jpn. J. Appl. Phys. **23**, 188 (1984).
[35] Y.-C. Li, Y.-H. Huang, C.-C. Huang, Y.-T. Liu, and C.-F. Pai, Phys. Rev. Appl. **20**, 024032 (2023).
[36] A. U. Canbolat, H. Sevinçli, and Ö. Çakır, Phys. Rev. B **106**, 104409 (2022).